



OPEN ACCESS

EDITED BY

Song Ma,
Chinese Academy of Sciences (CAS), China

REVIEWED BY

Wei Shen,
Anhui University of Chinese Medicine, China
Lisi Xie,
Sun Yat-sen Memorial Hospital, China

*CORRESPONDENCE

Liyang Ma,
✉ maliyangbz@163.com
Jiajing Zhang,
✉ jjiajing_z@bzmc.edu.cn

RECEIVED 27 December 2023

ACCEPTED 24 January 2024

PUBLISHED 12 February 2024

CITATION

Wang R, Li H, Han L, Han B, Bao Y, Fan H, Sun C, Qian R, Ma L and Zhang J (2024), Combining photodynamic therapy and cascade chemotherapy for enhanced tumor cytotoxicity: the role of CTT₂P@B nanoparticles. *Front. Bioeng. Biotechnol.* 12:1361966. doi: 10.3389/fbioe.2024.1361966

COPYRIGHT

© 2024 Wang, Li, Han, Han, Bao, Fan, Sun, Qian, Ma and Zhang. This is an open-access article distributed under the terms of the [Creative Commons Attribution License \(CC BY\)](https://creativecommons.org/licenses/by/4.0/). The use, distribution or reproduction in other forums is permitted, provided the original author(s) and the copyright owner(s) are credited and that the original publication in this journal is cited, in accordance with accepted academic practice. No use, distribution or reproduction is permitted which does not comply with these terms.

Combining photodynamic therapy and cascade chemotherapy for enhanced tumor cytotoxicity: the role of CTT₂P@B nanoparticles

Rongyi Wang, Hongsen Li, Lu Han, Boao Han, Yiting Bao, Hongwei Fan, Chaoyue Sun, Ruijie Qian, Liyang Ma* and Jiajing Zhang*

School of Pharmacy, Binzhou Medical University, Yantai, China

The mitochondria act as the main producers of reactive oxygen species (ROS) within cells. Elevated levels of ROS can activate the mitochondrial apoptotic pathway, leading to cell apoptosis. In this study, we devised a molecular prodrug named CTT₂P, demonstrating notable efficacy in facilitating mitochondrial apoptosis. To develop nanomedicine, we enveloped CTT₂P within bovine serum albumin (BSA), resulting in the formulation known as CTT₂P@B. The molecular prodrug CTT₂P is achieved by covalently conjugating mitochondrial targeting triphenylphosphine (PPh₃), photosensitizer TPPOH₂, ROS-sensitive thioketal (TK), and chemotherapeutic drug camptothecin (CPT). The prodrug, which is chemically bonded, prevents the escape of drugs while they circulate throughout the body, guaranteeing the coordinated dispersion of both medications inside the organism. Additionally, the concurrent integration of targeted photodynamic therapy and cascade chemotherapy synergistically enhances the therapeutic efficacy of pharmaceutical agents. Experimental results indicated that the covalently attached prodrug significantly mitigated CPT cytotoxicity under dark conditions. In contrast, TPPOH₂, CTT₂, CTT₂P, and CTT₂P@B nanoparticles exhibited increasing tumor cell-killing effects and suppressed tumor growth when exposed to light at 660 nm with an intensity of 280 mW cm⁻². Consequently, this laser-triggered, mitochondria-targeted, combined photodynamic therapy and chemotherapy nano drug delivery system, adept at efficiently promoting mitochondrial apoptosis, presents a promising and innovative approach to cancer treatment.

KEYWORDS

mitochondria-targeting, photodynamic therapy, bovine serum albumin, camptothecin, ROS-responsive

1 Introduction

Based on the most recent Global Cancer Statistics 2020 report, cancer has emerged as a primary or secondary factor contributing to mortality among individuals below the age of 70 in 112 nations worldwide (Sung et al., 2021). Chemotherapy, a conventional cancer treatment modality, often induces significant side effects due to its limited therapeutic specificity, bioavailability, and vulnerability to multidrug resistance (Li et al., 2018; Pan

et al., 2021; Zou et al., 2021). Prodrugs provide a technique to accomplish targeted drug activation at the site of the tumor, liberating bioactive medications as needed in order to minimize overall toxicity. Prodrug activation mainly relies on utilizing distinct characteristics of the tumor microenvironment, such as reduced pH, glutathione concentrations, hypoxia, and specific enzyme expression. Additionally, external stimuli like light, heat, and ultrasound can also be employed for this purpose (Yin et al., 2019). Red and near-infrared light are attractive stimuli for prodrug activation due to their deep tissue penetration depth and low phototoxicity.

Phototriggered prodrugs have shown great potential in tumor treatment, given their non-invasive and remote spatiotemporal control capabilities, which are increasingly utilized in precision tumor treatment. When exposed to laser radiation, photosensitizers have the ability to produce significant amounts of reactive oxygen species (ROS) (O'Connor et al., 2009; Yi et al., 2018; Agwa et al., 2023; Yang et al., 2023; Yu et al., 2023). These ROS can eliminate cancer cells and break down ROS-sensitive chemical bonds, such as thioketal (TK) (Shi et al., 2018), alkyl thioether or selenide (Luo et al., 2019), aryl boronic acid or ester (Daum et al., 2017). Utilizing ROS-sensitive bonds to covalently link chemotherapeutic drugs and photosensitizers in the design of photo-triggered molecular prodrugs improves the specificity of chemotherapy drugs, reduces side effects, and synchronizes drug distribution *in vivo* (Liu et al., 2016; Xu et al., 2016; Jiang et al., 2020; Lebepe et al., 2021). However, despite allowing temporal and spatial control of drug release, diverse release sites within the cell can significantly impact drug therapeutic efficacy. Therefore, exploring strategies to optimize therapeutic outcomes is imperative.

Mitochondria, which are versatile organelles that control cellular bioenergy, calcium balance, redox equilibrium, and programmed cell death, are responsible for 90% of intracellular ROS generation (Nunnari and Suomalainen, 2012; Yue et al., 2016a; Xie et al., 2020). Mitochondria possess antioxidant systems to maintain redox homeostasis, and ROS at specific concentrations benefit normal cellular physiological functions. However, excessive ROS disrupts redox equilibrium, inducing mitochondrial death (Porporato et al., 2018; Wang et al., 2023). The mitochondrial genome lacks an effective DNA damage repair mechanism, making it a sensitive target for drugs that act on DNA and reverse chemotherapy resistance (Mallick et al., 2018). The close proximity of the photosensitizer to the target area greatly enhances the effectiveness of photodynamic therapy, as a result of the brief lifespan and restricted spread of ROS in biological systems (<0.1 ms, <20 nm) (Yuan et al., 2014). Delivering chemotherapeutic medicines and photosensitizers to mitochondria maximizes treatment efficacy.

Here, we developed CTT₂P, a molecular prodrug targeting mitochondria. CTT₂P comprises a triphenylphosphine cation, a porphyrin-type photosensitizer, a ROS-sensitive bond thioketal (TK), and covalently coupled camptothecin (CPT). During cancer treatment, CPT, a typical medicine for the mitochondrial apoptosis pathway, acts as an inhibitor of cellular respiration and DNA topoisomerase I (Liu et al., 2019; Zhang et al., 2019; Chen et al., 2023). CPT was chosen as a chemotherapeutic drug to promote the generation of ROS and induce cell apoptosis in synergism with the photosensitizer laser-induced dual pathway. Positively charged

compounds are accumulated in the mitochondrial matrix of cancer cells due to their more negative membrane potential in the mitochondrial inner membrane compared to normal cells. With its excellent lipophilicity and positive charge, triphenylphosphine cation is a commonly utilized mitochondrial targeting group, facilitating rapid substance transport across the membrane to mitochondria (Mehta et al., 2017; Zielonka et al., 2017). Tumor cells, more sensitive to mitochondrial perturbations due to widespread metabolic reprogramming, benefit from prodrugs acting at the mitochondrial site, improving drug efficacy and efficiently promoting mitochondrial apoptosis, subsequently triggering cell apoptosis (Fu et al., 2019).

However, molecular prodrugs exhibit low solubility and are quickly metabolized in blood circulation, resulting in low bioavailability. Therefore, improving drug accumulation in tumor tissue becomes a practical consideration. Utilizing the enhanced permeability and retention (EPR) effect at the tumor site, nanoparticles (NPs) composed of either natural or synthetic substances efficiently administer a precise amount of molecular therapeutics to tumor tissue, proving to be an effective approach for drug delivery (Mayr et al., 2017; Luo et al., 2023).

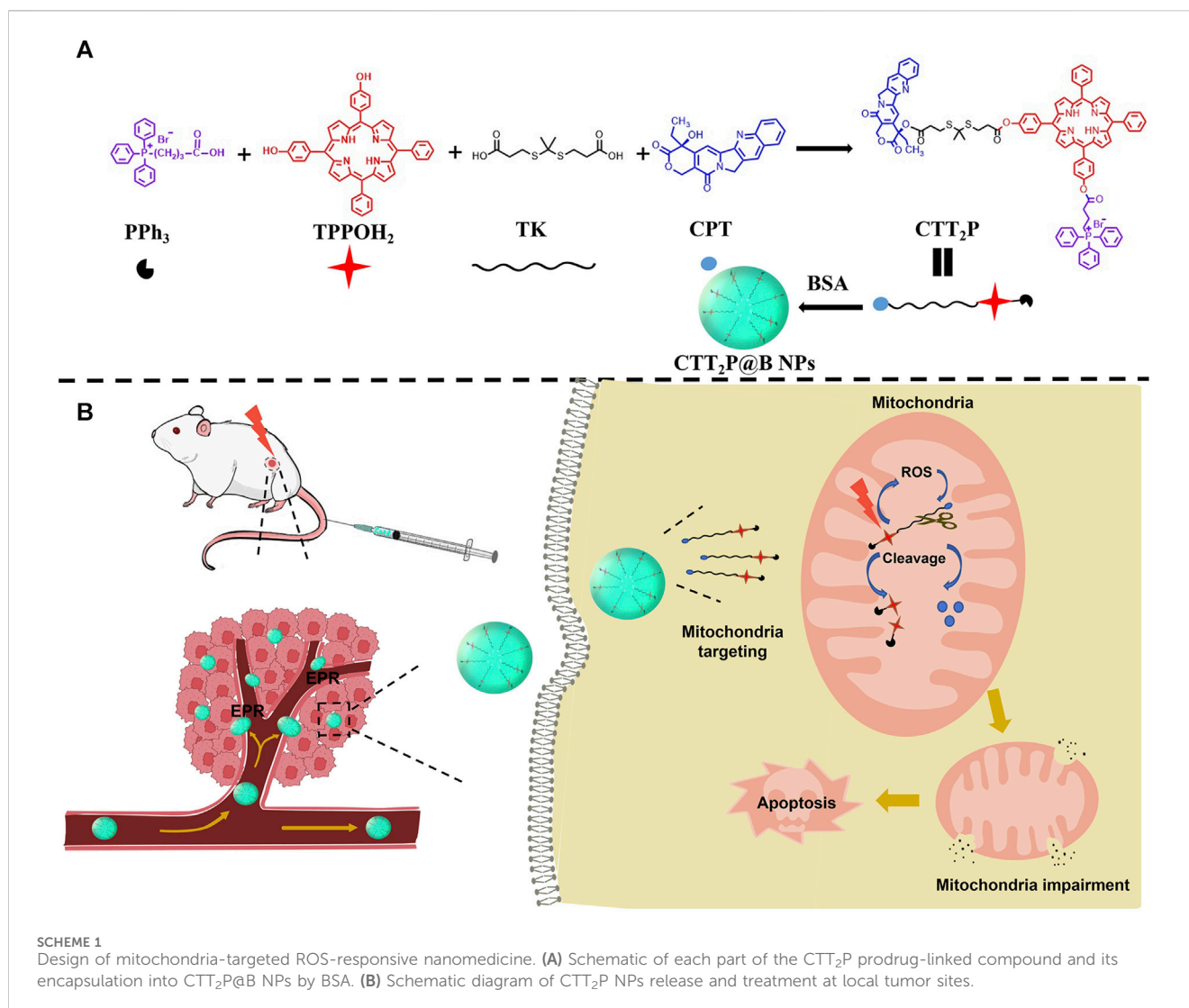
In this study, we created the molecular drug CTT₂P targeting mitochondria for ROS responsiveness (Scheme 1A, B). We encapsulated it through bovine serum albumin (BSA) as CTT₂P@BSA NPs to prolong drug circulation, delivering CTT₂P to the tumor site for maximal therapeutic efficacy with minimal side effects. First, CTT₂ was obtained by covalently linking the porphyrin derivative TPPOH₂ to the chemotherapeutic drug CPT using the ROS-sensitive bond TK. Derivating the 20-hydroxy group of CPT can decrease activity, reducing the side effects of chemotherapy drugs. (Hong et al., 2000). Then, triphenylphosphine PPh₃ was covalently linked to CTT₂ to achieve mitochondrial targeting of CTT₂P. Finally, a nano-drug delivery system (CTT₂P@B) was constructed by coating CTT₂P with bovine serum albumin (BSA). Triphenyl phosphate groups target CTT₂P to mitochondria after CTT₂P@B releases the prodrug CTT₂P in tumor cells. Low levels of ROS in tumor cells are insufficient to cleave TK bonds (Yin et al., 2019; Chu et al., 2020). However, irradiation with a 660 nm laser causes the photosensitizer component to generate ROS, significantly increasing ROS levels and enhancing cell damage.

Additionally, it cleaves the TK bond, releasing the photosensitizer and effective CPT in the mitochondria. CPT accumulation in mitochondria leads to ROS production (Zhang et al., 2019), increasing the breakage of the TK link and the cumulative release of CPT. This repeated superposition self-cycling action boosts mitochondrial apoptosis and triggers cell apoptosis with high efficiency and low toxicity.

2 Material and methods

2.1 Materials

Camptothecin (CPT), 3-mercaptopropionic acid, p-hydroxybenzaldehyde, benzaldehyde, 4-dimethylaminopyridine (DMAP), and 1,3-diphenylisobenzofuran (DPBF) were purchased from Shanghai Macklin Biochemical Technology Co., Ltd. (Shanghai, China). Pyrrole, 1-(3-dimethylaminopropyl)-3-



ethylcarbodiimide hydrochloride (EDCI), (3-carboxypropyl) triphenyl phosphonium bromide (PPh₃), and Bovine Serum Albumin (BSA) were purchased from Shanghai Aladdin Biochemical Technology Co., Ltd. (Shanghai, China). Propionic acid was purchased from Anhui Zesheng Technology Co., Ltd. (Shanghai, China). Mito-Tracker Green, Reactive Oxygen Species Assay Kit (DCFH-DA) was purchased from Beyotime Biotechnology Co., Ltd. (Shanghai, China). Annexin-V FITC/PI, Mitochondrial Membrane Potential Assay Kit (with JC-1) was purchased from Elabscience Biotechnology Co., Ltd. (Hubei, China). All other reagents were of analytical grade and used as received.

2.2 Synthesis of TK

The synthesis of thioketal (TK) was carried out according to established procedures (Yue et al., 2016b). Anhydrous acetone (5.70 g, 98.20 mmol) and 3-mercaptopropionic acid (5.21 g, 49.10 mmol) were thoroughly mixed, and anhydrous hydrogen chloride gas was introduced. The reaction proceeded for 4 h at

room temperature and was terminated. After crystallization in an ice water bath, the resulting product underwent filtration and was alternatively washed with hexane and cold water. Vacuum drying yielded the white powder product TK, with a 27.3% yield. Confirmation of TK was achieved through ¹H NMR spectroscopy (500 MHz, CDCl₃): δ 2.90 (t, 4H), 2.68 (t, 4H), 1.59 (s, 6H).

2.3 Synthesis of 5, 10-bis (4-hydroxyphenyl)-15, 20-diphenyl porphyrin (TPPOH₂)

For the synthesis of TPPOH₂, p-hydroxybenzaldehyde (45.00 mmol, 5.50 g) and benzaldehyde (45.00 mmol, 4.57 mL) were added to 150 mL of propionic acid and heated to reflux. Within a time frame of 20 min, Pyrrole (90.00 mmol, 6.23 mL) was introduced into a constant pressure funnel. The mixture was then stirred at a temperature of 140°C for a duration of 90 min. Following the reaction, vacuum concentration removed the propionic acid, producing an oily liquid. The liquid was dissolved in a mixture of dichloromethane and methanol (in a ratio of 70:1), then filtered. The resulting solution was concentrated under vacuum

to obtain the crude product. Separation and purification through silica gel column chromatography (100–200 mesh) with dichloromethane: methanol ratios of 50:1 and 100:1 yielded the purple product TPPOH₂, with a 2.4% yield. The confirmation was done using ¹H NMR (600 MHz, DMSO-d₆): δ 9.97 (s, 2H), 8.89 (s, 4H), 8.80 (s, 4H), 8.21 (d, J = 6.3 Hz, 4H), 8.01 (d, J = 8.2 Hz, 4H), 7.86–7.79 (m, 6H), 7.21 (d, J = 8.2 Hz, 4H), –2.90 (s, 2H), and ESI-MS: m/z calculated for C₄₄H₃₀N₄O₂ [M + H]⁺: 647.2441.

2.4 Synthesis of TK-CPT

The thioketal (TK) (10.08 mg, 0.04 mmol), 4-dimethylaminopyridine (DMAP) (5.86 mg, 0.048 mmol), and 1-(3-dimethylaminopropyl)-3-ethylcarbodiimide hydrochloride (EDCI) (9.20 mg, 0.048 mmol) were combined and added to 5 mL of dichloromethane in a concise process and stirred in an ice bath for 20 min. Subsequently, dropwise, 3 mL of dichloromethane-dissolved CPT (6.97 mg, 0.02 mmol) was meticulously added and stirred for 24 h at room temperature. Post-reaction, the solution underwent vacuum concentration to yield the resultant mixture. This mixture underwent separation and purification via silica gel column chromatography utilizing dichloromethane:methanol gradient elution ranging from 70:1 to 50:1. Ultimately, the white product TK-CPT was obtained with a yield of 40%. TK-CPT was confirmed using ¹H NMR and mass spectrometry (MS). ¹H NMR (600 MHz, DMSO-d₆): δ 8.70 (s, 1H), 8.13 (q, 2H), 7.87 (t, J = 7.6 Hz, 1H), 7.72 (t, J = 7.5 Hz, 1H), 7.24 (s, 1H), 5.50 (s, 2H), 5.32 (q, 2H), 2.94–2.76 (m, 4H), 2.69 (t, J = 7.2, 3.4 Hz, 2H), 2.38 (t, J = 7.0 Hz, 2H), 2.19–2.11 (m, 2H), 1.57 (s, 3H), 1.50 (s, 3H), 0.93 (t, J = 7.4 Hz, 3H). ESI-MS: m/z calculated for C₂₉H₃₀N₂O₇S₂ [M + H]⁺: 583.1565.

2.5 Synthesis of CTT₂

TK-CPT (11.65 mg, 0.02 mmol), DMAP (2.93 mg, 0.024 mmol), and EDCI (4.60 mg, 0.024 mmol) were included in 5 mL of dichloromethane and mixed in an ice bath for a duration of 20 min. After that, a solution of TPPOH₂ (25.87 mg, 0.04 mmol) dissolved in 4 mL of dichloromethane was added once, and the amalgamation reacted at room temperature for 24 h. Subsequently, the solution was subjected to vacuum concentration to obtain the resulting mixture. The resulting mixture was isolated and refined using a silica gel column chromatography method, employing a gradient elution of dichloromethane and methanol ranging from 100:1 to 70:1. Ultimately, the purple product CTT₂ was obtained with a commendable yield of 86%. CTT₂ was confirmed using ¹H NMR and mass spectrometry (MS). ¹H NMR (600 MHz, DMSO-d₆): δ 9.98 (s, 1H), 8.90 (d, J = 12.0 Hz, 2H), 8.80 (d, J = 13.6 Hz, 6H), 8.38 (s, 1H), 8.25–8.19 (m, 6H), 8.06 (d, J = 8.5 Hz, 1H), 8.01 (d, J = 8.3 Hz, 2H), 7.89 (d, J = 8.0 Hz, 1H), 7.86–7.80 (m, 6H), 7.77 (t, 1H), 7.57 (t, J = 7.5 Hz, 1H), 7.49 (d, J = 8.3 Hz, 2H), 7.25 (s, 1H), 7.21 (d, J = 8.4 Hz, 2H), 5.50 (s, 2H), 5.07 (q, 2H), 3.01–2.87 (m, 8H), 2.15 (q, J = 7.3 Hz, 2H), 1.68 (s, 3H), 1.63 (s, 3H), 0.94 (t, J = 7.4 Hz, 3H), –2.96 (s, 2H). ESI-MS: m/z calculated for C₇₃H₅₈N₆O₈S₂ [M + H]⁺: 1211.3829.

2.6 Synthesis of CTT₂P

(3-Carboxypropyl) triphenyl phosphonium bromide (PPh₃, 4.29 mg, 0.01 mmol), DMAP (1.47 mg, 0.012 mmol), and EDCI (2.30 mg, 0.012 mmol) were meticulously measured and introduced into 2 mL of dichloromethane and mixed in an ice bath for a duration of 20 min. Subsequently, 3 mL of CTT₂ (12.11 mg, 0.01 mmol) dissolved in dichloromethane was carefully added to the reaction solution, and the amalgamation underwent stirring for 24 h at room temperature. Post-reaction, the solution underwent vacuum concentration to yield the resultant mixture. This resultant mixture was separated and purified using silica gel column chromatography, employing a gradient elution of dichloromethane: methanol within the range of 70:1 to 20:1. Ultimately, the purple-black product CTT₂P was obtained, demonstrating a commendable yield of 66%. The structure of CTT₂P was confirmed using ¹H NMR and mass spectrometry (MS). ¹H NMR (600 MHz, DMSO-d₆): δ 8.93–8.71 (m, 8H), 8.38 (s, 1H), 8.27 (d, J = 8.2 Hz, 2H), 8.25–8.19 (m, 6H), 8.07 (d, J = 8.5 Hz, 1H), 7.97–7.89 (m, 10H), 7.87–7.81 (m, 12H), 7.78 (t, 1H), 7.62 (d, J = 8.3 Hz, 2H), 7.58 (t, J = 7.5 Hz, 1H), 7.50 (d, J = 8.3 Hz, 2H), 7.25 (s, 1H), 5.50 (s, 2H), 5.05 (q, 2H), 3.86–3.79 (m, 2H), 3.08–3.04 (m, 2H), 3.02–2.88 (m, 8H), 2.15 (q, J = 7.4 Hz, 2H), 2.09–2.00 (m, 2H), 1.68 (s, 3H), 1.63 (s, 3H), 0.94 (t, J = 7.4 Hz, 3H), –2.98 (s, 2H). ESI-MS: m/z calculated for C₉₅H₇₈N₆O₉S₂P⁺Br[–] [M-Br]⁺: 1541.4982.

2.7 ROS response test of CTT₂P

10 mg of CTT₂P was dissolved in d₆-DMSO and irradiated with a 280 mW cm^{–2}, 660 nm laser for 1 min and 5 min, respectively. The ROS response of CTT₂P was observed using ¹H NMR.

2.8 Preparation of CTT₂P@B NPs

CTT₂P@B NPs were synthesized using a desolvation method. Specifically, 15 mg of Bovine Serum Albumin (BSA) was dissolved in 1 mL of deionized water. After stirring to achieve complete dissolution, the pH was accurately set to 9.0 by adding a 0.1 M NaOH solution. Afterwards, a solution of CTT₂P dissolved in acetone, measuring 4 mL, was added to the aqueous phase at a steady rate of 1 mL min^{–1}, while keeping the stirring rate at 500 r·min^{–1}. After stirring for 30 min, 10 μL of 8% glutaraldehyde was incorporated, and the solution underwent a curing process for 12 h. Finally, the solution was centrifuged at 12,000 rpm for 20 min. The resulting precipitate was subjected to two additional resuspension and centrifugation with deionized water. The supernatant was retained, and the precipitate was re-dispersed in 2 mL of deionized water before being stored at 4°C.

2.9 Transmission electron microscopy observation and size distribution

The Zetasizer nanoZS (Malvern Instruments) was used to determine the particle size and zeta potential of the nanomedicine CTT₂P@B NPs. Furthermore, the shape of CTT₂P@B NPs was observed using the TEM (JEM-1400 microscope).

2.10 EE and DL of CTT₂P@B NPs

UV-vis spectroscopy was used to measure the absorbance of the supernatant, which was retained after centrifugation, at 415 nm. From the standard curve of CTT₂P, the calculation of CTT₂P@B NPs' encapsulation efficiency and drug loading was determined.

EE% = weight of drug in nanoparticles/weight of total drug × 100%

DL% = weight of drug in nanoparticles/weight of nanoparticles × 100%

2.11 Properties of spectra

The absorbance of TPPOH₂, CTT₂, CTT₂P, and CTT₂P@B in DMSO was measured using UV-vis spectroscopy. The fluorescence emission spectra of TPPOH₂, CTT₂, CTT₂P, and CTT₂P@B under 420 nm excitation were measured using a multifunctional microplate reader.

2.12 *In Vitro* drug release study

In vitro release assays were conducted employing a centrifugation-based methodology. CTT₂P@B NPs were evenly distributed in 1.5 mL of PBS (pH 7.4 and 5.0) containing 10% ethanol. Subsequently, they were placed in a constant-temperature shaker and incubated at 37°C. The nanosuspension was subjected to centrifugation at 12,000 r·min⁻¹ for 10 min at specific time intervals (0.25, 0.5, 1, 2, 4, 6, 8, 10, 12, 24, 36, and 48 h), and 1 mL of supernatant was collected and supplemented with 1 mL of fresh buffer. Quantifying the CTT₂P drug within the supernatant was executed utilizing UV-vis spectroscopy, facilitating the computation of the release rate at each designated time point.

2.13 *In Vitro* drug singlet oxygen detection

Solutions of TPPOH₂, CTT₂, CTT₂P, and CTT₂P@B NPs, each with a concentration of 5 μM and containing DPBF, were prepared. The DPBF concentration was set at 150 μg mL⁻¹. Subsequently, a 2 mL sample solution was placed in a 24-well plate. In order to commence the experiment, every specimen was exposed to light with a wavelength of 660 nm and an intensity of 280 mW cm⁻² for a duration of 16 min. UV-vis spectroscopy at 420 nm was diligently recorded at 1-min intervals throughout the irradiation period. The manifestation of generated singlet oxygen was indicated by the discernible reduction in DPBF absorption at 420 nm.

2.14 Cell culture and cellular ROS detection during irradiation

The murine breast cancer cells (4T1) were procured from Icell Biotech Co., Ltd. (Shanghai, China). The 4T1 cells were cultivated in Dulbecco's Modified Eagle's Medium (DMEM) supplemented with 10% (v/v) fetal bovine serum (FBS) and 1% (v/v) penicillin/streptomycin. The cells were cultivated in a

cell incubator maintained at a temperature of 37°C with 5% CO₂ (v/v).

To conduct experiments, 4T1 cells were placed in 12-well plates with a density of 1.5 × 10⁵ cells per well. After incubating for 24 h, the 4T1 cells were treated with 5 μM CPT, TPPOH₂, CTT₂, CTT₂P, and CTT₂P@B NPs individually for a duration of 6 h. Afterwards, the cells were treated with 10 μM DCFH-DA for a duration of 20 min, followed by a PBS wash. Subsequently, the cells were subjected to laser irradiation at a wavelength of 660 nm and intensity of 280 mW cm⁻² for a period of 1 min. The intracellular production of ROS was visualized using fluorescence microscopy.

2.15 Subcellular Co-localization experiment

The intracellular localization of different categories of drugs was examined using Confocal Laser Scanning Microscopy (CLSM). In summary, 4T1 cells were grown in confocal dishes with a cell density of 50,000 cells per well. After 24 h of incubation, the existing medium was removed, and TPPOH₂, CTT₂, CTT₂P, and CTT₂P@B NPs (with a photosensitizer concentration of 10 μM), diluted in fresh medium, were introduced. Afterwards, Mito-tracker Green (200 nM) was added to all samples and incubated together in fresh medium for 30 min to mark the mitochondria. In the end, the liquid was removed, cells were washed with PBS, and a small amount of new liquid was introduced to each well prior to being placed under CLSM for observation. The excitation wavelength and emission spectra for each fluorescence index were as follows: TPPOH₂, CTT₂, CTT₂P, and CTT₂P@B NPs were excited at 405 nm, with fluorescence emission spectra collected at 600–660 nm. Mito-Tracker Green was excited at 488 nm, and fluorescence emission spectra were collected from 510 to 540 nm.

2.16 Mitochondrial membrane potentials assay

Mitochondrial depolarization in 4T1 cells was assessed employing the JC-1 probe. Briefly, 4T1 cells were placed in 12-well plates with a concentration of 2 × 10⁵ cells per well. After being incubated at 37°C for 24 h, the cells were subjected to 5 μM of CPT, TPPOH₂, CTT₂, CTT₂P, and CTT₂P@B NPs for a duration of 6 h. Then, the cells were exposed to a 660 nm, 280 mW cm⁻² laser for 1 min, followed by an additional 18-h incubation period. The control group cells were treated with medium or carbonyl cyanide m-chlorophenyl hydrazone (CCCP) to ascertain the status of the membrane potential whether it remained normal or dissipated. Following the incubation period, the cells were rinsed with PBS, trypsinized, and then gathered in centrifuge tubes to be centrifuged. Afterward, 500 μL of JC-1 working solution were introduced and left to incubate at a temperature of 37°C for a duration of 20 min. After centrifugation, the liquid portion was discarded, and the cells were washed and centrifuged once using JC-1 Assay Buffer. Finally, the cells were resuspended to create a cell suspension. Flow cytometry analysis was performed using 525 nm (FITC channel) and 585 nm (PE channel) bandpass filters, with excitation at 488 nm.

2.17 Cytotoxicity test

4T1 cells were seeded in 96-well plates at a concentration of 5,000 cells per well using 100 μL of culture medium and incubated for 24 h. Afterwards, the cells were treated with different solutions of CPT, TPPOH₂, CTT₂, CTT₂P, and CTT₂P@B NPs (drug loading concentrations of 0.5, 1, 2, 5, 10, and 20 μM). For dark toxicity assessment, cells were exposed to drugs for a period of 24 h while being protected from any light exposure. For the assessment of phototoxicity, the cells underwent exposure to a laser with a wavelength of 660 nm and power density of 280 $\text{mW}\cdot\text{cm}^{-2}$ for a duration of 1 min, following continuous culturing for 6 h. After the irradiation, the cells were further cultured for 18 h. Then, a combination of CCK-8 and DMEM medium was introduced and incubated with the cells for 2 h, and the absorbance at 450 nm was determined using a microplate reader.

2.18 Cell apoptosis assay

4T1 cells were seeded in 6-well dishes with a density of 5×10^5 cells per well and incubated for 24 h. The cells were treated with CPT, TPPOH₂, CTT₂, CTT₂P, and CTT₂P@B NPs solutions (drug concentration of 5 μM) for 6 h. Following that, a laser with a wavelength of 660 nm and an intensity of 280 $\text{mW}\cdot\text{cm}^{-2}$ was used for 1 min of irradiation. The culture was then allowed to continue for 18 h post-irradiation. After two washes with PBS, the plates were trypsinized without EDTA, and the cells were collected in centrifuge tubes for centrifugation. Binding Buffer was added after resuspending and washing the single-cell suspensions with PBS. After being treated with Annexin-V FITC and PI for a duration of 15 min, the cells underwent evaluation of apoptosis using a flow cytometer (BD Canto II).

2.19 Hemolysis assay

Blood was obtained from mice, and erythrocytes were separated by centrifugation. The erythrocytes were subsequently diluted by washing with PBS before use. The red blood cell suspension was mixed with 10 μM solutions of CPT, TPPOH₂, CTT₂, CTT₂P, and CTT₂P@B NPs in the experiments. After incubation at 37°C for 2 h, the samples were centrifuged to collect the supernatant, which was then subjected to UV-vis spectroscopy analysis at 540 nm. PBS and Triton X-100 served as the negative and positive controls, respectively. Hemolysis was calculated using the following formula:

$$\text{Hemolysis (\%)} = \frac{(\text{OD}_{\text{sample}} - \text{OD}_{\text{negative}})}{(\text{OD}_{\text{positive}} - \text{OD}_{\text{negative}})} \times 100\%$$

2.20 Animal and tumor models

All Balb/c mice (4 weeks old, female) were procured from Jinan Pengyue Experimental Animal Breeding Co., Ltd. All animal studies followed the guidelines and protocols approved by the Animal Care Agency of Binzhou Medical University. The 4T1 tumor-bearing mouse model was established by subcutaneously injecting a 4T1 cell

suspension (1×10^6 cells) into the right abdomen of the mice. Mice were utilized for biodistribution and NIR fluorescence imaging studies when the tumor volume reached 200 mm^3 . Antitumor therapy was conducted using mice that had a tumor volume of 100 mm^3 .

2.21 *In Vivo* fluorescence imaging

The 4T1 tumor-bearing mice had their skin shaved and were divided into three groups randomly ($n = 3$ in each group). The mice were intravenously injected with 200 μL of CTT₂P and CTT₂P@B NPs (both containing 100 μg CTT₂P). Mice were anesthetized and imaged using the IVIS Spectrum (Perkin-Elmer, United States) at 2, 4, 8, 10, and 24 h after injection. The imaging involved an excitation wavelength of 640 nm and a fluorescence emission wavelength of 700 nm. After 24 h post-injection, the mice, as mentioned above, were euthanized, and major organs were collected and imaged.

2.22 *In Vivo* anti-tumor efficacy

In each group, the mice with 4T1 tumors were randomly divided into six groups ($n = 5$) and given NS or CPT, TPPOH₂, CTT₂, CTT₂P, and CTT₂P@B NPs intravenously. Each group was administered a single dose every other day, which is equal to a CPT dosage of 2 $\text{mg}\cdot\text{kg}^{-1}$ Cel. After 10 h of injection, the tumors in the laser irradiation groups were subjected to a 660 nm laser for a duration of 1 min, with a power intensity of 280 $\text{mW}\cdot\text{cm}^{-2}$. Subsequently, the therapeutic efficacy of each group was assessed by measuring tumor size every 2 days. The formula for calculating tumor volume is tumor volume (mm^3) = $(W^2 \times L)/2$, where L denotes the greater diameter of the tumor and W denotes the lesser diameter of the tumor. After 12 days, the mice were euthanized and their organs (including the heart, liver, spleen, lung, and kidney) along with solid tumor tissues were removed for histological examination. The examination was conducted using the standard H&E staining method. TUNEL immunohistochemical stains were performed to analyze tumor tissue apoptosis.

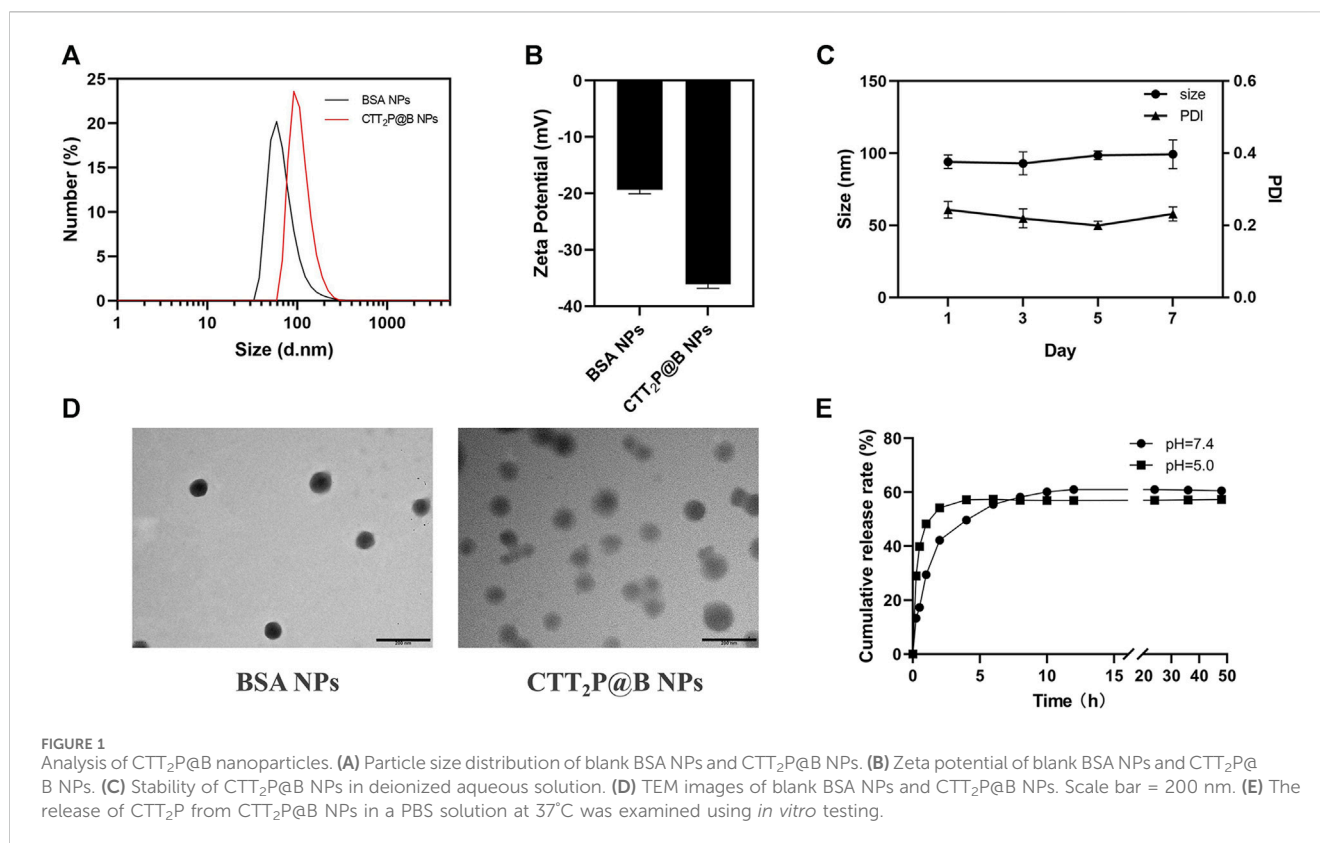
2.23 Statistical analysis

The mean \pm SD was used to express the quantitative data. The statistical analysis was performed utilizing the software GraphPad Prism 8.0. To compare two groups, the Student's t-test was used, while for comparing multiple groups, a one-way analysis of variance (ANOVA) was employed. Statistical significance was determined for p -values below 0.05 ($*p < 0.05$, $**p < 0.01$, $***p < 0.001$, $****p < 0.0001$).

3 Results and discussion

3.1 Synthesis and characterization of prodrug nanoparticles

The molecular prodrug CTT₂P is primarily synthesized through a three-step reaction (Supplementary Scheme S1). To begin with, TPPOH₂ and the TK sensitive to ROS were created using the

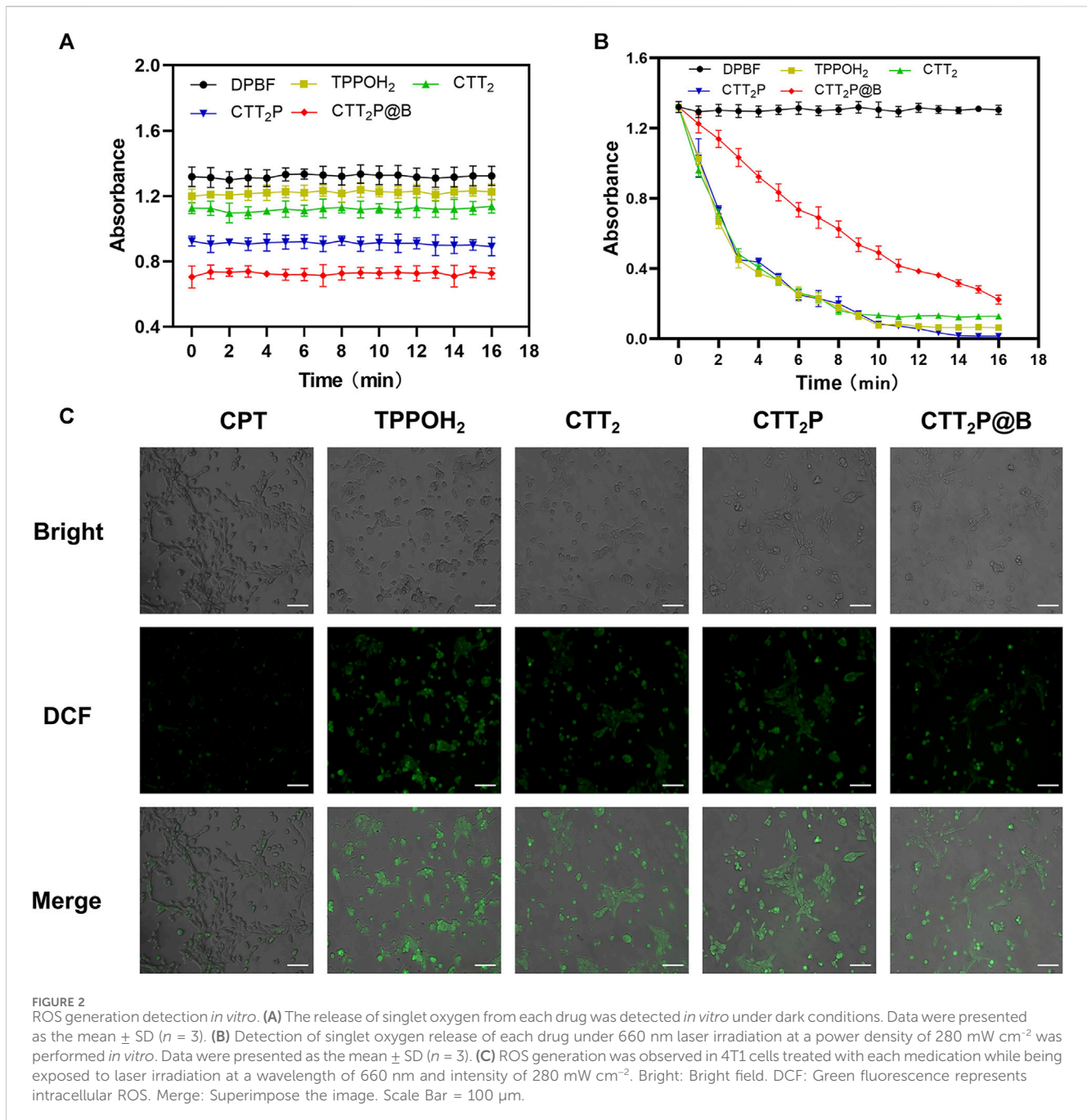


method described in the source. The structures of these compounds were validated through ¹H NMR and ESI-MS analyses (Supplementary Figures S1–S3). Subsequently, CTT₂, a novel ROS-cleavable compound, was synthesized by covalently coupling CPT with TPPOH₂ using TK. Finally, the molecular prodrug CTT₂P was synthesized from (3-carboxypropyl) triphenyl phosphonium bromide and CTT₂ through an esterification reaction. The structures of the described compounds were confirmed through ¹H NMR and ESI-MS analyses (Supplementary Figures S4–S9). We then measured the ROS response release for CTT₂P. Supplementary Figure S10 illustrates a significant reduction in the NMR peak of the TK part of CTT₂P after 1 min and 5 min of illumination, and a significant shift in the chemical shift of the CPT part of CTT₂P. This indicates that there is enough ROS for the compound CTT₂P to break TK bonds when exposed to a 280 mW cm⁻², 660 nm laser for 5 min.

The prodrug, which is bound covalently, reduces the escape of the drug while it circulates throughout the body, guaranteeing a one-to-one ratio between the target and the administered drug *in vivo*. Due to its positive charge, the triphenylphosphine group facilitates targeting the mitochondria of cancer cells. Upon exposure to laser light, TK in CTT₂P is cleaved, releasing CPT in response to the abundant ROS generated by the photosensitizer and those present in the mitochondria themselves. Hydrophobic CPT was selected as the chemotherapeutic drug not only for its anticancer activity and ease of modification but also for its ability to inhibit cellular respiration, leading to an excessive production of ROS in mitochondria (Sen et al., 2004). Conversely, the excessive ROS produced by photosensitizers and CPT can effectively induce mitochondrial apoptosis, triggering cell apoptosis.

We employed desolvation to encapsulate CTT₂P into BSA nanoparticles, yielding CTT₂P@B NPs. To validate the successful synthesis of CTT₂P@B, blank BSA NPs were synthesized as a control using the same method. The size and distribution of hydrated particles in blank BSA NPs and CTT₂P@B NPs were first measured using dynamic light scattering (DLS) (Figures 1A,B). The results revealed that the hydrated particle sizes of blank BSA NPs and CTT₂P@B NPs were 64.35 ± 5.09 nm and 92.89 ± 4.06 nm, respectively. Additionally, the potentials of blank BSA NPs and CTT₂P@B NPs were -19.37 ± 0.70 mV and -36.13 ± 0.68 mV, respectively. The CTT₂P@B NPs exhibited a size approximately 28 nm more prominent than the blank BSA NPs, and the potential had an absolute value of approximately 17 mV higher. These notable changes in particle size and potential indicated the successful encapsulation of CTT₂P in BSA.

Furthermore, as indicated by prior research, the higher the magnitude of the potential, the increased stability of the nanoparticles was observed (Khan et al., 2016). This implies that CTT₂P@B NPs exhibited enhanced stability compared to blank BSA NPs. Notably, the negatively charged surface of the NPs enhances their resistance to nonspecific protein adsorption in the bloodstream, ultimately prolonging their circulation time, as observed in other studies (Yuan et al., 2012). The results obtained from transmission electron microscopy (TEM) were consistent with the measured hydrated particle size using dynamic light scattering, confirming that CTT₂P@B NPs are indeed more significant than their blank BSA counterparts (Figure 1D). All these indicators strongly suggest the successful encapsulation of CTT₂P in BSA. TEM analysis revealed that CTT₂P@B NPs exhibited a uniform distribution and good



morphology, appearing as spherical particles. Subsequently, we evaluated the stability of CTT₂P@B NPs in an aqueous solution. As shown in Figure 1C, The dimensions and polydispersity index (PDI) of CTT₂P@B NPs remained stable over the course of 1 week, suggesting exceptional nanoparticle stability.

Utilizing the UV-vis spectroscopy of CTT₂P, the standard curve was used to determine the encapsulation efficiency and drug loading of CTT₂P@B NPs. The CTT₂P@B NPs exhibited an encapsulation efficiency of 43.98% \pm 2.38% and a drug loading of 2.75% \pm 0.15%. Next, we measured the spectral properties of TPPOH₂, CTT₂, CTT₂P, and CTT₂P@B (Supplementary Figures S11, S12). As observed in the UV spectra, the maximum absorbance of TPPOH₂, CTT₂, and CTT₂P around 420 nm gradually decreased

with the successive modification of chemical bonds. However, due to BSA encapsulation, CTT₂P@B exhibits a BSA UV absorption peak around 280 nm, and the maximum absorbance at 420 nm is smaller than that of CTT₂P. Similarly, based on the fluorescence emission patterns, the maximum emission wavelengths of TPPOH₂, CTT₂, CTT₂P, and CTT₂P@B gradually decreased. Additionally, we examined the drug release pattern of CTT₂P@B NPs in simulated physiological and tumor-acidic conditions. The drug release rate of CTT₂P@B NPs in PBS solutions with pH values of 7.4 and 5.0 was evaluated by examining the cumulative release over time (Figure 1E), the results indicated a faster drug release under acidic conditions. This accelerated release is attributed to BSA's self-degradation and erosion in acidic environments, aligning with

our designed system. In the acidic environment of tumor cells, CTT₂P@B NPs can more readily release the molecular drug CTT₂P into tumor cells, facilitating the effective targeting of mitochondria and the intended therapeutic function.

3.2 *In Vitro* detection of ROS

1,3-Diphenylisobenzofuran (DPBF) can react with singlet oxygen (¹O₂) generated during the process. The absorption intensity of DPBF at 420 nm decreases with an increase in the concentration of ¹O₂ (Xu et al., 2018). Hence, DPBF functioned as a tool for assessing the ability of medications to produce singlet oxygen (¹O₂). Initially, we examined whether there was ¹O₂ release from the drug under dark conditions. In Figure 2A, based on the data, it is clear that the DPBF, TPPOH₂, CTT₂, CTT₂P, and CTT₂P@B NPs did not show any noticeable alterations in absorbance when kept in darkness. This suggests that the photosensitizer created did not generate ¹O₂ without light. We confirmed the release of ¹O₂ from the synthesized photosensitizer under laser irradiation by utilizing the absorbance change of the drug in the dark as a control. Figure 2B shows that the absorbance of DPBF also did not undergo significant changes under laser irradiation conditions, indicating that the presence of DPBF did not interfere with the experiment. The slope and degree of absorbance drop represent the rate of ¹O₂ production. The slopes of TPPOH₂, CTT₂, and CTT₂P are nearly identical, suggesting a consistent rate of ¹O₂ release and an excellent ability to produce ¹O₂. However, the slope of absorbance decline for CTT₂P@B NPs was slower than TPPOH₂, CTT₂, and CTT₂P. The presence of nanoparticles leads to a decrease in the rate of ¹O₂ emission, resulting in a reduction of laser irradiation intensity.

Additionally, DCFH-DA staining was utilized to analyze the generation of intracellular ROS in 4T1 cells across all drug groups. DCFH-DA, an impermeable indicator of cellular permeability for reactive oxygen species (ROS), is hydrolyzed by esterases within cells and then oxidized by ROS to generate the fluorescent compound DCF. As observed through a fluorescence microscope (Figure 2C), the CPT group did not display noticeable fluorescence. In contrast, the TPPOH₂, CTT₂, CTT₂P, and CTT₂P@B NPs groups exhibited significant fluorescence, indicating that drugs modified with a photosensitizer still retained the ability to generate ROS upon irradiation in cells.

3.3 Evaluation of mitochondrial targeting function

To assess the drugs' capacity to target mitochondria, the drugs were administered to 4T1 cells for a duration of 6 h, and the colocalization of the drug was analyzed using CLSM. Since our drugs were explicitly designed for mitochondrial targeting, we assessed mitochondrial localization (Figure 3A) through fluorescent double staining. We utilized the Mito-Tracker Green, a fluorescent probe for mitochondria, along with the red fluorescence emitted by our designed drugs. The yellow area in the overlapping images indicates the colocalization of the photosensitizer with Mito-Tracker Green. The results revealed that cells treated with CTT₂P and CTT₂P@B

NPs exhibited clear colocalization with Mito-Tracker Green, in contrast to TPPOH₂ and CTT₂. However, the CTT₂P@B NPs displayed a more pronounced yellow area than CTT₂P alone, as the nanodrugs were more easily taken up by the cells, resulting in increased drug accumulation in the mitochondria. This observation aligns with our design concept; CTT₂P and CTT₂P@B NPs demonstrate effective mitochondrial localization, targeting the mitochondria upon entering tumor cells under the influence of triphenylphosphine groups.

Next, we evaluated drug-induced impairment of mitochondria in every group by examining the potential of mitochondrial membrane using the positively charged dye JC-1. Prior research has shown that the JC-1 probe is effective in identifying mitochondrial harm. In normal mitochondria, the green monomers of JC-1 can enter the cytoplasm and accumulate, forming numerous red J-aggregates. A change in fluorescence color from red to green suggests the presence of membrane potential decline and considerable damage to the mitochondria (Zhang et al., 2019). Therefore, we quantified mitochondrial damage in 4T1 cells induced by each drug using flow cytometry. The green fluorescence channel (FITC) represented "J-monomer," while the red fluorescence channel (PE) represented "J-aggregate." As illustrated in Figure 3B, after being exposed to laser, the CPT, TPPOH₂, CTT₂, CTT₂P, and CTT₂P@B NPs groups experienced a decrease in mitochondrial membrane potential (in the right lower quadrant) with loss rates of 35.8%, 19.1%, 40.1%, 52.8%, and 62.1%, respectively. The data indicate that CPT can induce moderate mitochondrial dysfunction, which is consistent with previous reports (Sen et al., 2004). Meanwhile, triphenylphosphine-modified CTT₂P caused more damage to mitochondria than TPPOH₂ and CTT₂ because it more easily accumulated at the mitochondrial site. CTT₂P@B NPs could enter cells more quickly and accumulate more drugs at the mitochondrial site, resulting in a higher rate of mitochondrial damage than the molecular drug CTT₂P.

3.4 *In Vitro* anti-tumor studies

Mitochondria play a vital role in cellular respiration and serve as a significant generator of reactive oxygen species (ROS). Therefore, drugs targeting mitochondria can achieve maximum therapeutic efficacy. In order to examine the *in vitro* anticancer properties of the synthesized medications, we first evaluated the toxic effects of different drugs on 4T1 cells through the CCK-8 assay. 4T1 cells were treated with CPT, TPPOH₂, CTT₂, CTT₂P, and CTT₂P@B NPs in the dark or under laser irradiation (Figures 4A,B). Under dark conditions, TPPOH₂, CTT₂, CTT₂P, and CTT₂P@B nanoparticles exhibited more than 80% cell viability at concentrations below 10 μM, showing minimal harm to cells in contrast to CPT. CTT₂ and CTT₂P enhance the stability of the CPT lactone ring and reduce cytotoxicity by modifying the 20-hydroxyl group of CPT. When the concentration of CTT₂, CTT₂P, and CTT₂P@B NPs was above 10 μM, CTT₂, and CTT₂P, as well as CTT₂P@B NPs, showed obvious cytotoxicity in the dark, but CTT₂P@B NPs showed less cytotoxicity than CTT₂P. This indicates that high concentrations of CTT₂, CTT₂P, and CTT₂P@B NPs still retain some cytotoxicity due to the presence of CPT under dark conditions. Simultaneously,

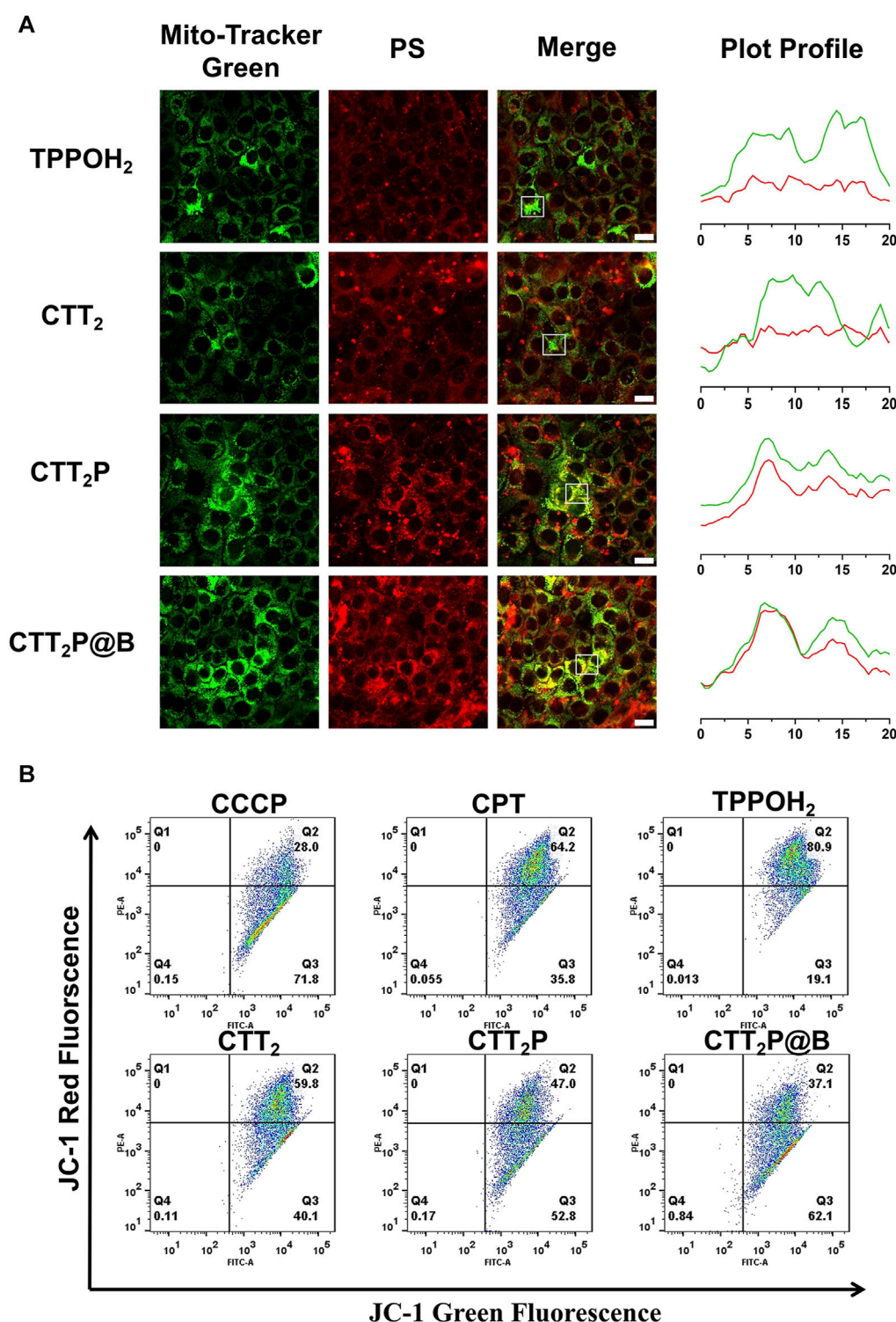
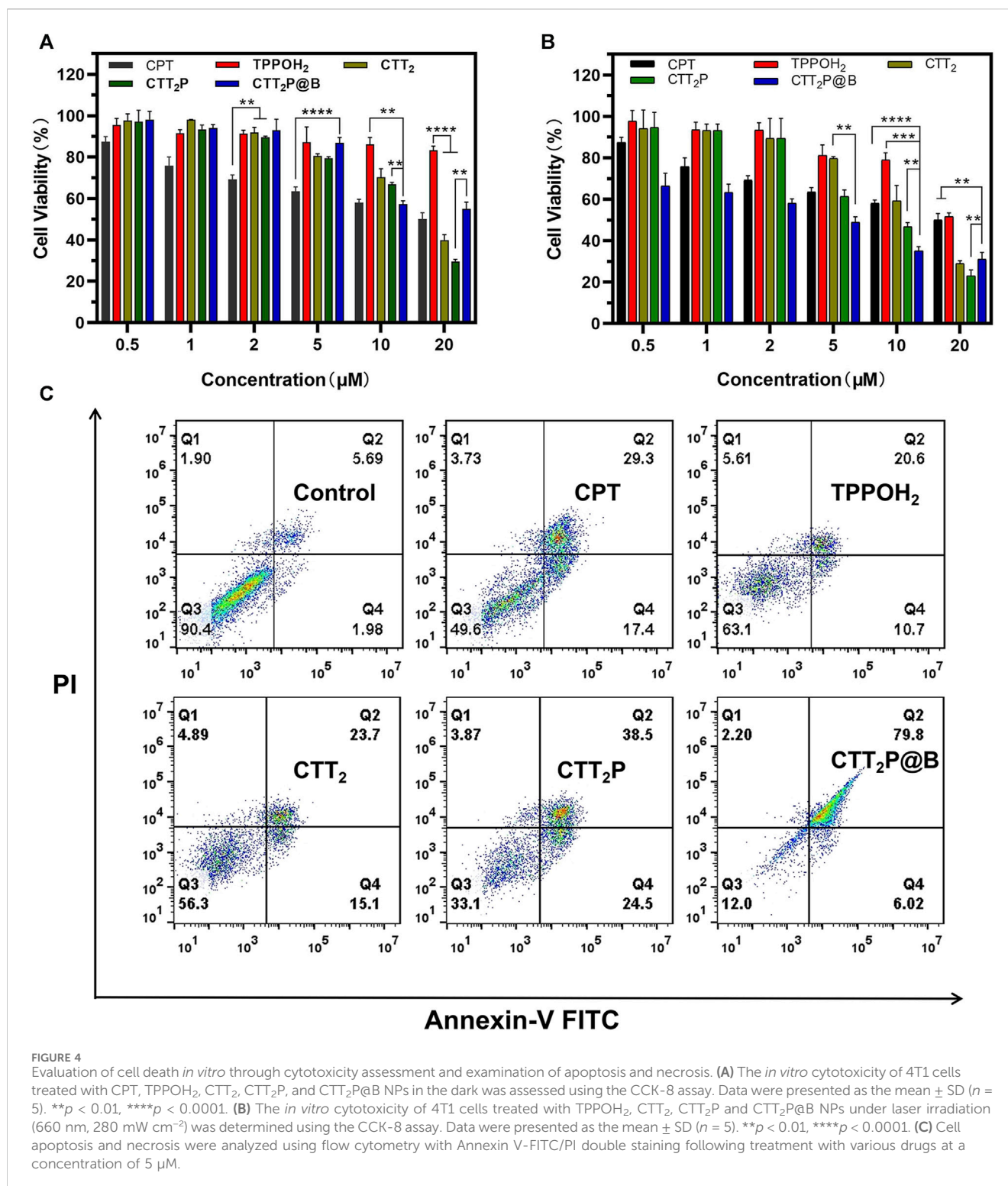


FIGURE 3 Evaluation of mitochondrial targeting function. **(A)** Confocal images of the mitochondrial sites of TPPOH₂, CTT₂, CTT₂P, and CTT₂P@B NPs in 4T1 cells. Mito-Tracker Green was used to stain the mitochondria in the green channel. The red channel was derived from the emission of the photosensitizer fraction (PS) itself. Merge stands for superimposed image. The Green and red curves in the Plot Profile represent the gray value of Mito-Tracker Green and PS, respectively. Scale bar = 20 μm. **(B)** Flow cytometry JC-1 method was used to analyze the mitochondrial function of cells treated with different drugs. Red fluorescence: normal mitochondria (J-aggregate); Green fluorescence: depolarized mitochondria (J-monomer).

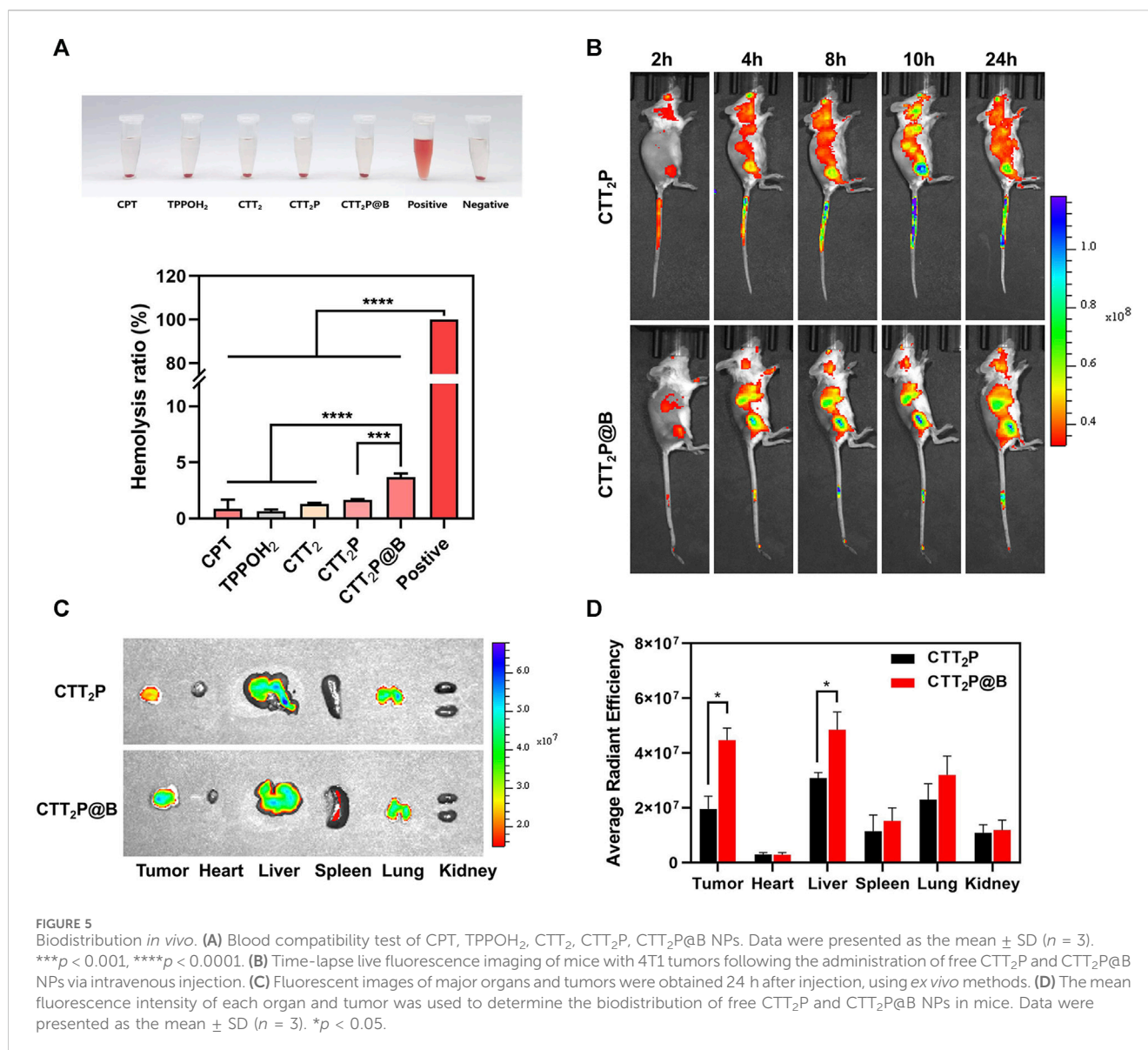
CTT₂P@B nanoparticles have the ability to decrease the cytotoxic effects of drugs by facilitating sustained release. When exposed to laser radiation (at a wavelength of 660 nm and intensity of

280 mW cm⁻²), TPPOH₂, CTT₂, CTT₂P, and CTT₂P@B NPs exhibited a significant reduction in cell viability compared to the CPT group. This indicates a dose-dependent and gradually escalating



cytotoxic effect. This suggests that ROS-induced TK breakdown and CPT release enhance cell damage, further amplified by drugs targeting mitochondria. Similarly to the results obtained in the dark, the cytotoxicity of a high concentration (20 μM) of CTT₂P@B NPs was reduced compared to CTT₂P. This reduction was attributed to the relatively small amount of drug accumulation caused by the high concentration of CTT₂P@B NPs.

Apoptosis rates, which include both early and late apoptosis, were examined through the use of the Annexin V-FITC/PI apoptosis detection kit and flow cytometry. As depicted in Figure 4C, laser-irradiated CTT₂P@B NPs induced a significantly higher apoptosis rate (85.82%) compared to that of free drugs CTT₂P (63%), CTT₂ (38.8%), TPPOH₂ (31.3%), and CPT (46.7%) under the same conditions. This result aligns with the trend observed in the



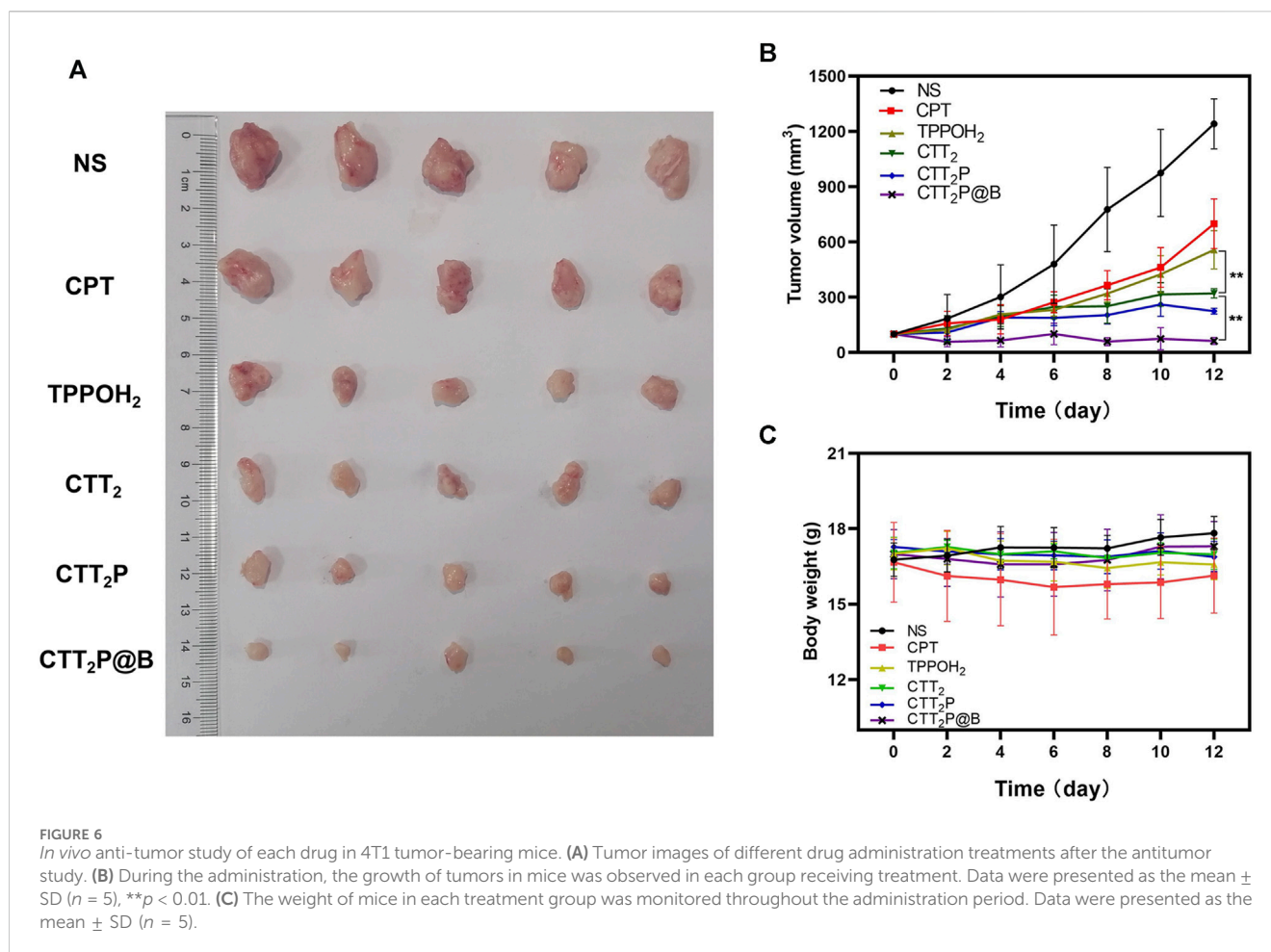
in vitro cytotoxicity results and indicates that the cytotoxicity of the drugs is associated with both early and late apoptosis. Furthermore, it confirms that the prodrug CTT₂P, modified with a mitochondrial targeting group, exhibits a more effective anti-tumor effect after being encapsulated with BSA.

3.5 *In Vivo* biodistribution

First, the hemolysis test verified the blood compatibility of each drug. As depicted in Figure 5A, the hemolysis rate of CPT, TPPOH₂, CTT₂, CTT₂P, and CTT₂P@B NPs at high concentrations did not exceed 5%. This indicates that the drugs exhibit good blood compatibility and can be safely administered via tail vein injection. We then investigated the biodistribution and drug delivery of CTT₂P and CTT₂P@B NPs in 4T1 tumor-bearing mice. CTT₂P, possessing near-infrared fluorescence, obviates the need for physical packaging with other dyes, allowing it to integrate

diagnosis and therapy. To monitor the distribution of medication in the body, an *in vivo* imaging system (IVIS) was utilized for fluorescence imaging. Images were captured at specific time intervals. As illustrated in Figure 5B and Supplementary Figure S13, higher accumulation was observed at the tumor site of mice treated with free CTT₂P at 10 h. However, no significant accumulation occurred at 24 h, indicating rapid clearance of free CTT₂P in mice.

On the other hand, CTT₂P@B NPs showed notable buildup after 4 h, which lasted until 24 h. The fluorescence intensity at the tumor location reached its peak approximately 10 h post-injection, suggesting the highest accumulation of CTT₂P@B NPs. Furthermore, *ex vivo* analysis of major organs and tumors was conducted 24 h post-injection to determine their distribution. As demonstrated in Figures 5C,D, in the heart and kidney of both groups, there were no apparent fluorescence signals, suggesting that neither drug group showed any signs of cardiotoxicity or nephrotoxicity. Liver and tumor tissues exhibited a notably



elevated signal in the CTT₂P@B NPs group compared to the free CTT₂P group. The enhanced fluorescence signal in the entire circulatory system and *ex vivo* tumor tissues at the exact CTT₂P dosage supports the long-circulating effect and tumor-targeting capabilities of CTT₂P@B NPs.

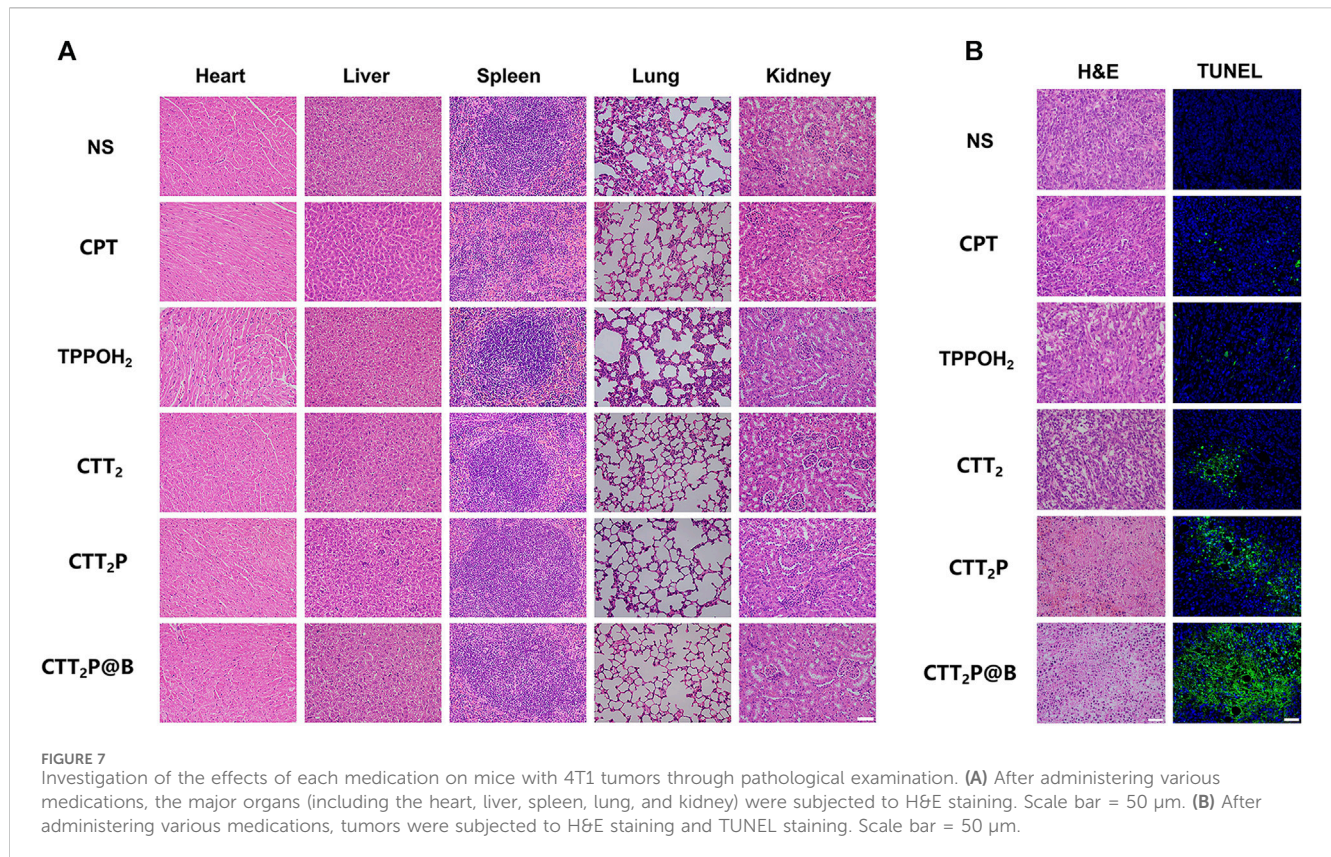
3.6 *In Vivo* anti-tumor studies

The therapeutic efficacy of various drug groups on 4T1-bearing mice was validated through tail vein injection of CPT at a dosage equivalent to 2 mg kg⁻¹. Based on the *in vivo* distribution results, laser irradiation was conducted 10 h after drug injection. Tumor images and tumor volume curves are depicted in Figures 6A,B. Tumor volume increased rapidly in mice treated with NS after laser irradiation, indicating an inability to impede tumor progression. The tumor volumes in the CPT and TPPOH₂ groups were comparable. However, the anti-tumor effect was inadequate, suggesting that neither chemotherapy nor photodynamic therapy alone could inhibit tumor growth. The CTT₂ group exhibited a more pronounced anti-tumor effect than the CPT and TPPOH₂ groups. However, it still fell short of the CTT₂P group, indicating that CTT₂P, a molecular drug targeting the mitochondrial region, may produce a more potent cascade effect and a more significant therapeutic impact due to its proximity to the target. Due to

enhanced blood circulation time and improved accumulation at the tumor site, the mice in the CTT₂P@B group exhibited the highest level of tumor inhibition and anti-tumor impact. The *in vivo* tumor-suppressing properties of TPPOH₂, CTT₂, CTT₂P, and CTT₂P@B NPs were enhanced when exposed to laser radiation, in line with the findings from *in vitro* tests on cell toxicity and programmed cell death. This further validates that the molecular drug CTT₂P, modified with a mitochondrial targeting group, exhibits superior therapeutic efficacy after encapsulation in BSA.

Furthermore, the mice's body weight and major organ tissue sections were analyzed using hematoxylin-eosin (H&E) staining to evaluate the biological safety of each treatment group. As depicted in Figure 6C, during the entire experimental period, there was no significant decrease in the weight of mice in any of the groups. The findings suggest that the medications in every category did not have any significant effect on the wellbeing of the mice. No histomorphological changes, bleeding, or infiltration of inflammatory cells were observed in the heart, liver, spleen, lung, and kidney sections stained with H&E in all groups (Figure 7A). This suggests that the current dosage of these medications is biologically safe.

The tumor tissues were evaluated for histopathological features using H&E staining (Figure 7B). Compared with the NS group, the tumor cells in each treatment group exhibited cell atrophy and nuclear pyknosis. The CTT₂P and CTT₂P@B NPs groups demonstrated more pronounced nuclear pyknotic phenomena



than the CPT, TPPOH₂, and CTT₂ groups. The apoptosis of tumor tissues was detected by terminal deoxynucleotidyl transferase-mediated dUTP-biotin nick end labeling (TUNEL) staining (Figure 7B), where blue represents living cells, and green represents apoptotic cells. The findings were consistent with the results of H&E staining. The absence of a notable disparity in cell apoptosis between the CPT group and the TPPOH₂ group suggests that the anti-tumor effect of single chemotherapy and photodynamic therapy is suboptimal. On the other hand, the TPPOH₂, CTT₂, CTT₂P, and CTT₂P@B NPs groups showed a gradual increase in apoptosis, leading to a significant rise in the count of cells undergoing apoptosis. This further validates the excellent anti-tumor effect of CTT₂P@B NPs.

4 Conclusion

In summary, we have successfully designed and synthesized a ROS-responsive prodrug, CTT₂P, demonstrating high efficacy in inducing mitochondrial damage and subsequent apoptosis. Furthermore, we have formulated CTT₂P@B NPs, encapsulating the prodrug CTT₂P within BSA for efficient delivery and controlled release. The photosensitizer is covalently linked to CPT through a ROS-sensitive bond, TK. Additionally, the mitochondrial targeting group, triphenylphosphine, is incorporated to create the covalently linked prodrug, CTT₂P. This covalent linkage enhances the specificity of chemotherapeutic drugs, minimizing side effects and

synchronizing their *in vivo* distribution. The CTT₂P@B NPs, formed by encapsulating the molecular prodrug CTT₂P with BSA, facilitate the transport and release of the drug to tumor cells. Guided by the triphenylphosphine group, the molecular prodrug CTT₂P selectively targets the mitochondrial site in tumor cells. Upon 660 nm laser irradiation, the photosensitizer component of the CTT₂P prodrug generates a significant amount of ROS. These ROS induce mitochondrial damage and cleave the ROS-sensitive group TK in the prodrug. Furthermore, the accumulated CPT in the mitochondrial region exerts its chemotherapeutic action, generating additional ROS that disrupt the respiratory chain and promote mitochondrial apoptosis. Ultimately, through the synergistic effects of photodynamic therapy using a photosensitizer and chemotherapy with CPT, these drugs effectively enhance mitochondrial apoptosis, leading to cell apoptosis. The CTT₂P@B molecular prodrug delivery system demonstrates low toxicity and a remarkable ability to induce mitochondrial apoptosis under laser irradiation. The findings of this research offer valuable information on the potential of organelle-specific methods to trigger apoptosis in cancerous cells.

Data availability statement

The original contributions presented in the study are included in the article/Supplementary Material, further inquiries can be directed to the corresponding authors.

Ethics statement

The animal study was approved by the Biomedical Research Ethics Committee of Binzhou Medical University (Ethics Section 2023 No. 205). The study was conducted in accordance with the local legislation and institutional requirements.

Author contributions

RW: Data curation, Formal Analysis, Investigation, Methodology, Writing—original draft, Writing—review and editing. HL: Investigation, Writing—original draft. LH: Investigation, Writing—original draft. BH: Investigation, Writing—original draft. YB: Investigation, Writing—original draft. HF: Investigation, Writing—original draft. CS: Investigation, Writing—original draft. RQ: Investigation, Writing—original draft. LM: Formal Analysis, Methodology, Writing—review and editing. JZ: Formal Analysis, Funding acquisition, Methodology, Writing—review and editing.

Funding

The author(s) declare financial support was received for the research, authorship, and/or publication of this article. We are grateful for financial support from the National Natural Science

References

- Agwa, M. M., Elmotasem, H., Elsayed, H., Abdelsattar, A. S., Omer, A. M., Gebreel, D. T., et al. (2023). Carbohydrate ligands-directed active tumor targeting of combinatorial chemotherapy/phototherapy-based nanomedicine: a review. *Int. J. Biol. Macromol.* 239, 124294. doi:10.1016/j.ijbiomac.2023.124294
- Chen, Z., Huang, Q., Song, Y., Feng, X., Zeng, L., Liu, Z., et al. (2023). Cubosomes-assisted transdermal delivery of doxorubicin and indocyanine green for chemophotothermal combination therapy of melanoma. *Biomed. Pharmacother.* 166, 115316. doi:10.1016/j.biopha.2023.115316
- Chu, B., Qu, Y., He, X., Hao, Y., Yang, C., Yang, Y., et al. (2020). ROS-Responsive camptothecin prodrug nanoparticles for on-demand drug release and combination of chemotherapy and photodynamic therapy. *Adv. Funct. Mat.* 30 (52). doi:10.1002/adfm.202005918
- Daum, S., Reshetnikov, M. S. V., Sisa, M., Dumych, T., Lootsik, M. D., Bilyy, R., et al. (2017). Lysosome-targeting amplifiers of reactive oxygen species as anticancer prodrugs. *Angew. Chem. Int. Ed.* 56 (49), 15545–15549. doi:10.1002/anie.201706585
- Fu, A., Hou, Y., Yu, Z., Zhao, Z., and Liu, Z. (2019). Healthy mitochondria inhibit the metastatic melanoma in lungs. *Int. J. Biol. Sci.* 15 (12), 2707–2718. doi:10.7150/ijbs.38104
- Hong, Z., Chyi, L., Prakash, S., Yun, H. C., Michelle, B., Annapurua, P., et al. (2000). 20-O-Acylcamptothecin derivatives: evidence for lactone stabilization. *J. Org. Chem.* 65 (15), 4601–4606. doi:10.1021/jo000221n
- Jiang, M., Mu, J., Jacobson, O., Wang, Z., He, L., Zhang, F., et al. (2020). Reactive oxygen species activatable heterodimeric prodrug as tumor-selective nanotheranostics. *ACS Nano* 14 (12), 16875–16886. doi:10.1021/acsnano.0c05722
- Khan, M. A., Zafaryab, M., Mehdi, S. H., Ahmad, I., and Rizvi, M. M. (2016). Characterization and anti-proliferative activity of curcumin loaded chitosan nanoparticles in cervical cancer. *Int. J. Biol. Macromol.* 93 (Pt A), 242–253. doi:10.1016/j.ijbiomac.2016.08.050
- Lebepe, T. C., Parani, S., Ncapayi, V., Maluleke, R., Mbaz, G. I. M., Fanoro, O. T., et al. (2021). Graphene oxide-gold nanorods nanocomposite-porphyrin conjugate as promising tool for cancer phototherapy performance. *Pharmaceuticals* 14 (12), 1295. doi:10.3390/ph14121295
- Li, N., Sun, Q., Yu, Z., Gao, X., Pan, W., Wan, X., et al. (2018). Nuclear-targeted photothermal therapy prevents cancer recurrence with near-infrared triggered copper sulfide nanoparticles. *ACS Nano* 12 (6), 5197–5206. doi:10.1021/acsnano.7b06870
- Foundation of China (No. 22001020), Foundation of Binzhou Medical University (No. 2019KYQD23) and Yantai Medical Antibacterial Material Innovation Service Platform.

Conflict of interest

The authors declare that the research was conducted in the absence of any commercial or financial relationships that could be construed as a potential conflict of interest.

Publisher's note

All claims expressed in this article are solely those of the authors and do not necessarily represent those of their affiliated organizations, or those of the publisher, the editors and the reviewers. Any product that may be evaluated in this article, or claim that may be made by its manufacturer, is not guaranteed or endorsed by the publisher.

Supplementary material

The Supplementary Material for this article can be found online at: <https://www.frontiersin.org/articles/10.3389/fbioe.2024.1361966/full#supplementary-material>

- death in unicellular hemoflagellate *Leishmania donovani*. *Cell Death Differ.* 11 (8), 924–936. doi:10.1038/sj.cdd.4401435
- Shi, S., Zhang, L., Zhu, M., Wan, G., Li, C., Zhang, J., et al. (2018). Reactive oxygen species-responsive nanoparticles based on PEGlated prodrug for targeted treatment of oral tongue squamous cell carcinoma by combining photodynamic therapy and chemotherapy. *ACS Appl. Mat. Interfaces* 10 (35), 29260–29272. doi:10.1021/acsami.8b08269
- Sung, H., Ferlay, J., Siegel, R. L., Laversanne, M., Soerjomataram, I., Jemal, A., et al. (2021). Global cancer Statistics 2020: GLOBOCAN estimates of incidence and mortality worldwide for 36 cancers in 185 countries. *CA Cancer J. Clin.* 71 (3), 209–249. doi:10.3322/caac.21660
- Wang, C., Yang, X., Qiu, H., Huang, K., Xu, Q., Zhou, B., et al. (2023). A co-delivery system based on chlorin e6-loaded ROS-sensitive polymeric prodrug with self-amplified drug release to enhance the efficacy of combination therapy for breast tumor cells. *Front. Bioeng. Biotechnol.* 11, 1168192. doi:10.3389/fbioe.2023.1168192
- Xie, L., Shi, F., Li, Y., Li, W., Yu, X., Zhao, L., et al. (2020). Drp1-dependent remodeling of mitochondrial morphology triggered by EBV-LMP1 increases cisplatin resistance. *Signal Transduct. Target Ther.* 5 (1), 56. doi:10.1038/s41392-020-0151-9
- Xu, F., Liu, M., Li, X., Xiong, Z., Cao, X., Shi, X., et al. (2018). Loading of indocyanine green within polydopamine-coated laponite nanodisks for targeted cancer photothermal and photodynamic therapy. *Nanomaterials* 8 (5), 347. doi:10.3390/nano8050347
- Xu, Q., He, C., Xiao, C., and Chen, X. (2016). Reactive oxygen species (ROS) responsive polymers for biomedical applications. *Macromol. Biosci.* 16 (5), 635–646. doi:10.1002/mabi.201500440
- Yang, F., Xu, M., Chen, X., and Luo, Y. (2023). Spotlight on porphyrins: classifications, mechanisms and medical applications. *Biomed. Pharmacother.* 164, 114933. doi:10.1016/j.biopha.2023.114933
- Yi, G., Hong, S. H., Son, J., Yoo, J., Park, C., Choi, Y., et al. (2018). Recent advances in nanoparticle carriers for photodynamic therapy. *Quant. Imaging. Med. Surg.* 8 (4), 433–443. doi:10.21037/qims.2018.05.04
- Yin, W., Ke, W., Chen, W., Xi, L., Zhou, Q., Mukerabigwi, J. F., et al. (2019). Integrated block copolymer prodrug nanoparticles for combination of tumor oxidative stress amplification and ROS-responsive drug release. *Biomaterials* 195, 63–74. doi:10.1016/j.biomaterials.2018.12.032
- Yu, C., Kong, L., Tian, J., Zhang, Y., Jia, X., Dang, W., et al. (2023). Photoacoustic imaging-guided triple-responsive nanoparticles with tumor hypoxia relief for improving chemotherapy/photothermal/photodynamic synergistic therapy against breast cancer. *Biomed. Pharmacother.* 164, 114928. doi:10.1016/j.biopha.2023.114928
- Yuan, Y., Liu, J., and Liu, B. (2014). Conjugated-polyelectrolyte-based polyprodrug: targeted and image-guided photodynamic and chemotherapy with on-demand drug release upon irradiation with a single light source. *Angew. Chem. Int. Ed.* 53 (28), 7163–7168. doi:10.1002/anie.201402189
- Yuan, Y. Y., Mao, C. Q., Du, X. J., Du, J. Z., Wang, F., and Wang, J. (2012). Surface charge switchable nanoparticles based on zwitterionic polymer for enhanced drug delivery to tumor. *Adv. Mat.* 24 (40), 5476–5480. doi:10.1002/adma.201202296
- Yue, C., Yang, Y., Zhang, C., Alfranca, G., Cheng, S., Ma, L., et al. (2016a). ROS-responsive mitochondria-targeting blended nanoparticles: chemo- and photodynamic synergistic therapy for lung cancer with on-demand drug release upon irradiation with a single light source. *Theranostics* 6 (13), 2352–2366. doi:10.7150/thno.15433
- Yue, C., Zhang, C., Alfranca, G., Yang, Y., Jiang, X., Yang, Y., et al. (2016b). Near-infrared light triggered ROS-activated theranostic Platform based on Ce6-CPT-UCNPs for simultaneous fluorescence imaging and chemo-photodynamic combined therapy. *Theranostics* 6 (4), 456–469. doi:10.7150/thno.14101
- Zhang, W., Hu, X., Shen, Q., and Xing, D. (2019). Mitochondria-specific drug release and reactive oxygen species burst induced by polyprodrug nanoreactors can enhance chemotherapy. *Nat. Commun.* 10 (1), 1704. doi:10.1038/s41467-019-09566-3
- Zielonka, J., Joseph, J., Sikora, A., Hardy, M., Ouari, O., Vasquez-Vivar, J., et al. (2017). Mitochondria-targeted triphenylphosphonium-based compounds: syntheses, mechanisms of action, and therapeutic and diagnostic applications. *Chem. Rev.* 117 (15), 10043–10120. doi:10.1021/acs.chemrev.7b00042
- Zou, W., Hao, J., Wu, J., Cai, X., Hu, B., Wang, Z., et al. (2021). Biodegradable reduce expenditure bioreactor for augmented sonodynamic therapy via regulating tumor hypoxia and inducing pro-death autophagy. *J. Nanobiotechnology* 19 (1), 418. doi:10.1186/s12951-021-01166-y